Proceedings of Global Power and Propulsion Society
ISSN-Nr: 2504-4400
GPPS Xi'an21
18th – 20th October, 2021
www.gpps.global

GPPS-TC-2021-#229

Study on Structural Strength and Air-tightness Analysis of a Large Axial Compressor Casing

Zhang Xiaolong
Xi'AnShaangu Power Co.
whoxlzhang@163.com
Xi'an,Shaanxi,China

Li Bing
Xi'an JiaotongUniversity
bli@xjtu.edu.cn
Xi'an,Shaanxi,China

Yuan Zhicai
Xi'AnShaangu Power Co.
yzc001637@shaangu.com
Xi'an,Shaanxi,China

Shen Zhen
Xi'AnShaangu Power Co.
920382696@qq.com
Xi'an,Shaanxi,China

Zhang Wushuai
Xi'AnShaangu Power Co.
ironsmith103@163.com
Xi'an,Shaanxi,China

Xu Jing
Xi'AnShaangu Power Co.
xujing23st@163.com
Xi'an,Shaanxi,China

Zhao Peng
Xi'AnShaangu Power Co.
nuaazp@163.com
Xi'an,Shaanxi,China

Chen Guang
Xi'AnShaangu Power Co.
chen_guang_cg@126.com
Xi'an,Shaanxi,China

ABSTRACT

Axial-flow compressor is a kind of large-scale air compressor, of which the casing is themain component. Accessories such as seals, bearing housings, adjustment mechanisms, and couplings are mounted on the compressor casing. Operated under various extreme temperature conditions, the reliability and working efficiency of the compressor aredirectly affected by the structural rigidity, strength, and air-tightness of the compressor casing. In the context of this problem, the FEA software ANSYS was used to calculate the temperature pattern, deformation field, and stress field of the casing under working conditions, hydrotest, and assembly state.Further, study the rigidity, strength and air-tightness of the casing. The rationality of the simplified analysis model is verified by the actual hydrotest data. The results of this analysis show that under all conditions, the deformation of the casing is within the acceptable range. After eliminating abnormal stress of local spot, the stress of all regions is lower than the yield limit of the material. The structural rigidity and strength of the casing are sufficient. The clearance between most splitting surfacesof the flange is less than 1mm, which is in accordance with the working condition of the sealing strip. These analysis results provide a theoretical basis and design reference for the structural design of the casing of this type of axial-flow compressor.

INTRODUCTION

The axial compressor is a large air compressor whose casing is welded casing. The engineering practice has the following three requirements for the compressor casing: sufficient rigidity to avoid excessive deformation due to excessive gas temperature or pressure; sufficient strength to withstand the stress caused by gas pressure and temperature difference; the flange joint surface should be tight to ensure that the gas will not leak to the outside of the machine. In general design, the strength of the compressor casing is usually ensured by qualitatively increasing safety factors, which results in a heavy casing, a long design period, and unsatisfactory optimization effects. In addition, for a long time, engineers have been improving the performance of the compressor mainly by improving and optimizing the rotator of the compressor-the impeller and blades, ignoring the calculation and research of stators, such as the casing. With the emergence of various advanced calculation means and methods, the difficulty of exploring the potential capabilities of static components has been reduced, and the analysis and improvement of their structures have been emphasized. In order to evaluate and improve the casing structure, it is necessary to obtain a large amount of data with the help of powerful finite element analysis tools as the basis for structural optimization[1, 2].

In this paper, the large-scale finite element software ANSYS Workbench is used to establish a high-precision finite element model for the casing of a large axial compressor, to carry out the analysis of the temperature field, deformation field and stress field of the casing under design conditions, hydrotest [3], and assembly conditions, and to check its rigidity, strength and air-tightness. The research work provides a theoretical basis and design reference for the strength and air-tightness design of the casing of this type of axial compressor.

ESTABLISHMENT OF THE FINITE ELEMENT MODEL OF CASING

In order to facilitate the division of the finite element mesh and the setting of boundary conditions, the original CAD model is reasonably simplified during modeling [4]. The simplified contents include:

1) Deletion of installation hooks, bolt holes thatdo not need to be analyzed, spotface of screw holes of the upper casing (retaining the bearing surface of the bolts), chamfering of screw holes of the lower casing, and fillet of the blade bearing cylinder;

2) Simplification of the details of the connection between the rib and the casing (deleting holes, fillets, etc.);

3) The bolts are established by beam elements, and the connection between the bolts and the upper and lower casings is established by point-to-surface contact.

Figure 1 Simplified casing model

There are a total of 186 M72 bolts in the above model. In the calculation of hydrotest and the analysis of design conditions, bolts are not the focus of an investigation but only serve as a carrier for applying bolt pre-tightening force, so it can be simplified, which will reduce the number of meshes greatly. According to the characteristics of finite element analysis and the functions of ANSYS Workbench software, the bolts are simplified into beam elements of circular cross-sections. As shown in Figure 2, the number of bolt nodes in a single solid element is 15,771, and the number of bolt nodes in a beam element is 28. The simplified bolt array is shown in Figure 2(b). Through the comparison calculation of the two kinds of bolts, it is found that with other conditions unchanged, the calculation results of the casings using solid bolts and beam element bolts are just slightly different, but the use of beam element bolts can greatly reduce the overall mesh number of the model and improve calculation efficiency [5]

(a) Solid element bolts(b) Beam element bolts

Figure 2 Actual bolt model (a) and simplified model (b)

The internal structure of the casing analyzed in this paper is irregular, and the air inlet and outlet surfaces are complicated. Therefore, a high-order tetrahedral element with intermediate nodes is selected for meshing, and a free division method is used to divide the mesh. First, according to the characteristic length of the structure in the model, the overall mesh size of the model is defined; according to the load and structural characteristics, mesh encryption is done for the loading plane, the split surface, the bearing surface of the screw hole, the contact surface of the blade bearing cylinder and the casing, used to improve the accuracy of analysis results. In addition, it is also necessary to edit the generated mesh so that the interconnected two parts of the solid mesh nodes can achieve one-to-one correspondence, and to merge the nodes at the welding point to avoid the settlement error caused by the mismatch of the mesh nodes [6-8].

The established finite element mesh model is shown in Figure 3. The model has 1.88 million nodes and 1.09 million elements.

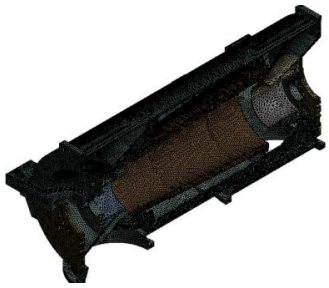

Figure 3 Meshing effect of the casing model

This research involves three materials: Q390C, ZG230-450 and 16Mn. The physical parameters of Q390C material are shown in Table 1, and the other two materials will not be repeated. The elastic modulus, thermal conductivity, linear expansion coefficient, and Poisson's ratio of all materials change with temperature[9]. This is an important basic data for finite element thermal analysis.

BOUNDARY CONDITIONS AND LOAD APPLICATION

This paper considers 11 kinds of working conditions, 1 kind of hydrotest, 1 kind of assembly state, a total of 13 kinds of analysis and calculations in different situations. The boundary conditions are same. Here is an introduction to the boundary conditions and load application methods under one of the working conditions:

Table 1 Q390C material physical properties

Material designation	**Q390C**		**Density** (kg/m^3)	7.84×10^3	
Temperature (℃)	Room temperature	100	200	300	400
Elastic modulus $E(10^3 MPa)$	213	208	201	194	185
Thermalconductivity $\lambda(W/(m \cdot K))$	-	39.6	43.0	41.7	39.9
Coefficient of linear expansion $\alpha_l(10^{-6}\ 1/K)$(at 20℃)	-	12.7	13.1	13.7	14.1
Poisson's ratio μ	0.283	0.275	0.275	0.278	0.276

(1) Constraint conditions: An upward circular surface is divided from the four cat's claws with the position of the cat's claw where bolts are mounted being the radius and the surface is used as the Z-axis constraint, which simulates the gravity situation of the cat's claws in the actual installation. The inner ring surfaces of the two cat's claws at the high-pressure end are used as the X-axis constraint, that is, the deformation in the X-axis direction of the casing takes the high-pressure end as the dead center. The middle screw hole of the low-pressure end plate is used as a Y-axis constraint. This constraint position is not the constraint position when the compressor is actually installed. It is only to ensure that the entire casing is symmetrically expanded on both sides with the Y-axis as the symmetrical axis during the calculation process.

(2) Component weight: bearing box on the intake side: 4000kg; bearing box on the exhaust side: 7000kg; adjusting cylinder: 10000kg; servo motor: 2000kg; rotor: 75000kg. The weight is applied to each installation surface as a uniform force perpendicular to the ground.

(3) Bolt pre-tightening force: The bolt size is M72, the smallest part of the bolt is 58.5mm in diameter, and the elastic modulus is about 200GPa (the 16Mn elastic modulus decreases slightly with the increase of temperature), if the bolt stretch is 1‰, then the calculated pre-tightening force is 530kN. The pre-tightening force is applied in two steps, the first step is loading, and the second step is locking.

(4) Pressure load: applying the corresponding pressure load to the inner wall of each cavity in the casing. Since the pressure in each cavity is small and there is a negative pressure (pressure is less than atmospheric pressure), the atmospheric pressure cannot be ignored, so the relative pressure is used here, that is, the absolute pressure minus the atmospheric pressure. Figure 4 shows the relative pressure of each cavity under a typical negative pressure condition.

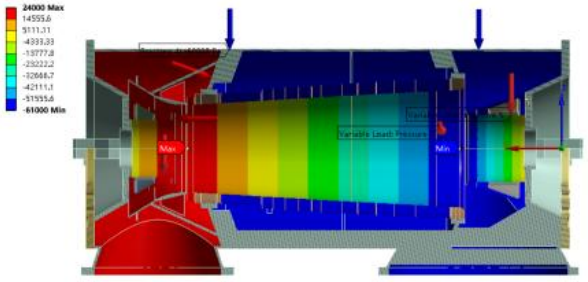

Figure 4 Pressure value (relative pressure, Pa) in the casing under a certain working condition

(5) Temperature load [7, 9]: according to the characteristics of temperature load, heat convection load is applied to the inner surface of the compressor, and the convective heat transfer coefficient: low-pressure cavity takes the empirical value of 100 W/m^2, high-pressure cavity takes an empirical value of 150 W/m^2;the inner surface of the blade bearing cylinder applies convective load according to the gradual value; the cavity between the blade bearing cylinder and the casing takes the natural convection heat transfer coefficient of 25 W/m^2, and the temperature takes the middle value of the intake and exhaust temperature. Convection load and radiation load are applied to the outer surface of the compressor, the room temperature is 25℃, and the natural convection heat transfer coefficient is 25 W/m^2.

RESULTS AND DISCUSSION

1) Hydrotest conditions

(1) Theoretical calculation

The water pressure is applied to the internal surface of the casing as shown in Figure 5, considering the gravity of the water and the self-weight of the casing.

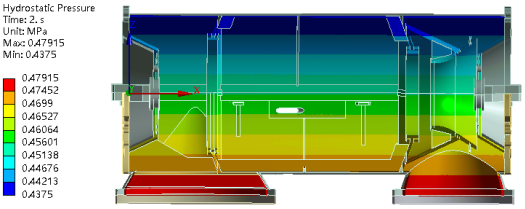

Figure 5 Water pressure distribution inside the casing

Figure 6 shows the cloud diagrams of the casing in all directions.

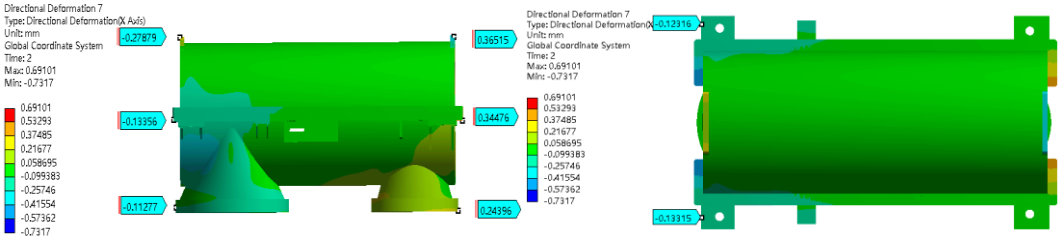

(a) Side view of casing deformation in X direction (mm)(b) Top view of casing deformation in X direction (mm)

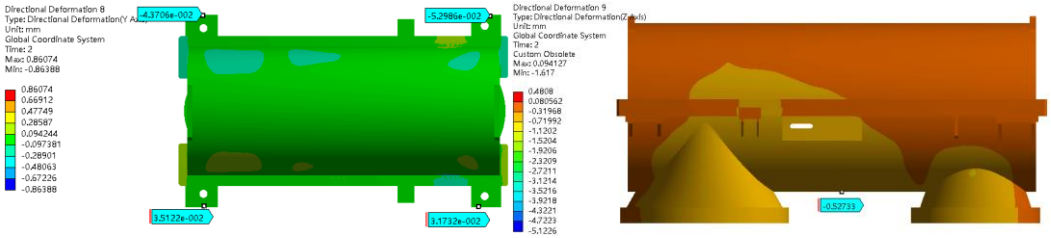

(c) Cloud diagram of casing deformation in Y direction (mm)(d) Cloud diagram of casing deformation in Z direction (mm)

Figure 6 Deformation cloud diagrams in various directions under hydraulic conditions

(2) Actual measurement of hydrotest

During the hydrotest of the casing, the deformation in all directions is monitored, and the actual measurement point arrangement is shown in Figure 7.

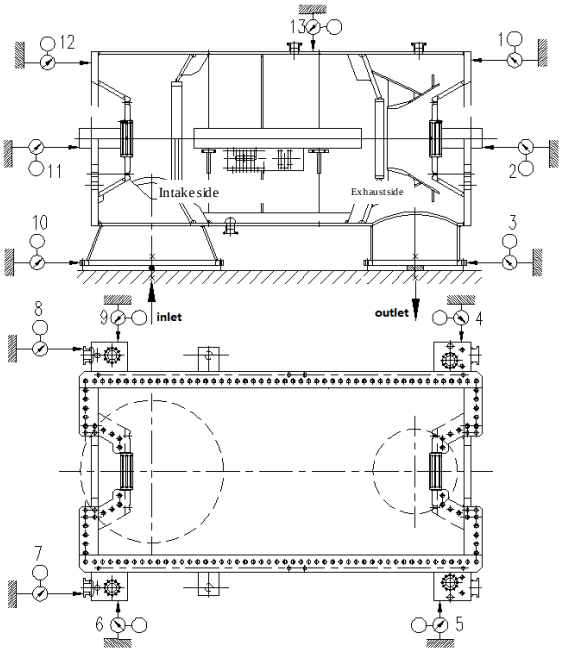

Figure 7Layout of hydrotest measuring points

(3) Comparison of theoretical calculation and actual measurement results

According to the theoretical calculation results of the hydrotest conditions and the measured monitoring point data, a comparison table is formed as shown in Table 2.

Table 2 Comparison table of theoretical and measured results

Measuring points	Theory (mm)	Actual measurement (mm)
1 (X direction)	0.36515	0.41
2 (X direction)	0.34476	0.3
3 (X direction)	0.24396	0.27
4 (Y direction)	-0.0529	-0.06
5 (Y direction)	0.03173	0.03
6 (Y direction)	0.03512	0.03
7 (X direction)	-0.13315	-0.14
8 (X direction)	-0.12316	-0.11
9 (Y direction)	-0.04371	-0.37
10 (X direction)	-0.11277	-0.1
11 (X direction)	-0.13356	-0.12
12 (X direction)	-0.27879	-0.3
13 (Z direction)	-0.52733	-0.57

It can be seen from Table 2 that the theoretical calculations under the hydrotest conditions of the casing are in good agreement with the measured results, which verifies that the casing finite element analysis model is reasonable.

2) Design conditions

Under a certain typical working condition, the calculation result of the casing temperature field is shown in Figure 8. Under this temperature field, the calculation results of its X-, Y-, and Z-direction deformation values are all shown in Figure 9. The stress distribution is shown in Figure 10. The sealing situation of the split surfaceis shown in Figure 11.

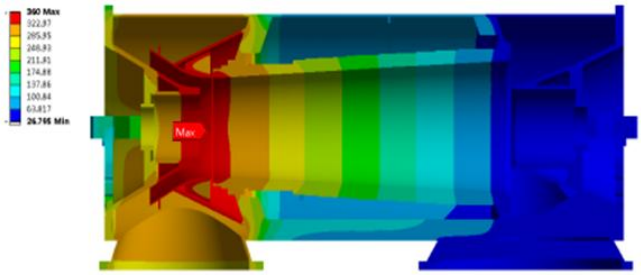

Figure 8 Casing temperature distribution diagram under a certain working condition (℃)

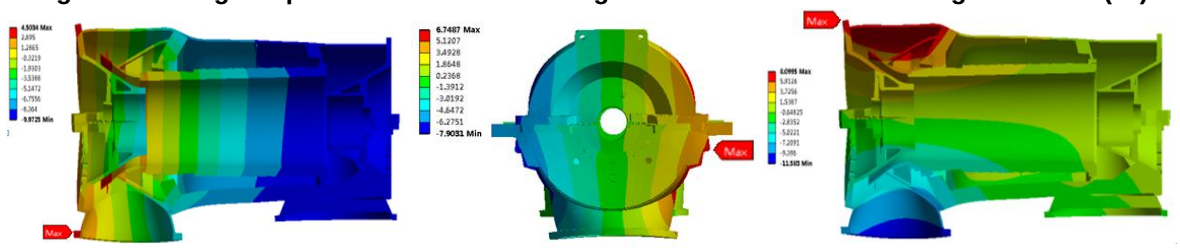

(a) X directiondeformation (mm)(b)Y direction deformation (mm)(c) Z direction deformation (mm)

Figure 9 Deformation of the casing under a certain working condition

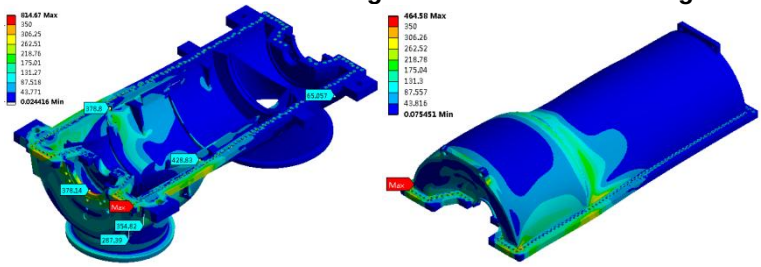

(a) Stress distribution of lower casing (MPa)(b) Stress distribution of upper casing (MPa)

Figure 10 Stress distribution under a certain working condition

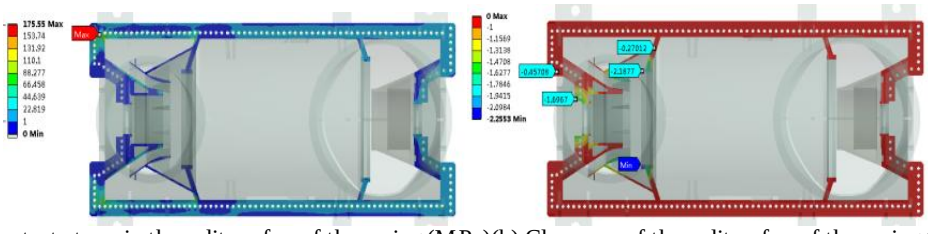

(a) Contact stress in the split surfaceof the casing (MPa)(b) Clearance of the splitsurfaceof the casing (mm)

Figure 11 The contact state of casing split surface under certain working condition

Table 3 lists the important calculation results of all calculations (Important results also include the casing stress distribution. However, due to the existence of local stress anomalies, the exact value of the true maximum stress cannot be determined, so it can only be observed and used in engineering analysis, and cannot be used for data analysis). From the data in the table and the comparison of the hot and cold end conditions in the cloud diagram of the calculation results, it can be concluded that under working conditions (negative pressure conditions and positive pressure conditions, not involving special conditions such as hydrotest and assembly conditions), the temperature gradient is the major reason for the large stress of the compressor casing and large split surface gap.

Figure 12 and Figure 13 respectively show the scatter plots of the relationship between the exhaust temperature and the overall maximum deformation value and the split surface gap under working conditions. It can be seen from Figure 12 that as the exhaust temperature rises, the maximum overall deformation becomes larger, and the two have a good linear relationship. It can be seen from Figure 13 that as the exhaust temperature rises, the split surface gap becomes larger, but the regularity is not as good as the relationship between the overall deformation value and the temperature. This is mainly due to the fact that the split surface gapis more sensitive to the setting of pressure, temperature and other boundary conditions, bolt pre-tightening force, component load and other factors, and the calculation is more difficult to converge. Based on the above results, it can be inferred that the operating temperature is the most important consideration in the design of the casing of the axial compressor. The decisive factor of the core indicators such as the maximum deformation value, the maximum stress, and the split surface gap is the casing temperature.

Table 3 Summary of all calculation results

Calculation	Situation description	Exhaust pressure Kpa(A)	Exhaust temperature ℃	Overall deformation mm	Split surfacegap mm
1	Negative pressure conditions	14	280	9.7	1.80
2	Negative pressure conditions	105	285	9.9	1.59
3	Negative pressure conditions	115	214	7.2	1.30
4	Negative pressure conditions	14	309	10.8	1.94
5	Negative pressure conditions	105	290	10.1	1.55
6	Negative pressure conditions	105	223	7.5	1.38
7	Negative pressure conditions	14	360	12.7	2.52
8	Negative pressure conditions	105	309	10.8	1.57
9	Negative pressure conditions	118	251	8.7	1.35
10	Negative pressure conditions	125	360	12.7	2.19
11	Positive pressure conditions	750	280	9.9	0.62
12	Assembly status (no bolts)	101	25	0.5	0.55

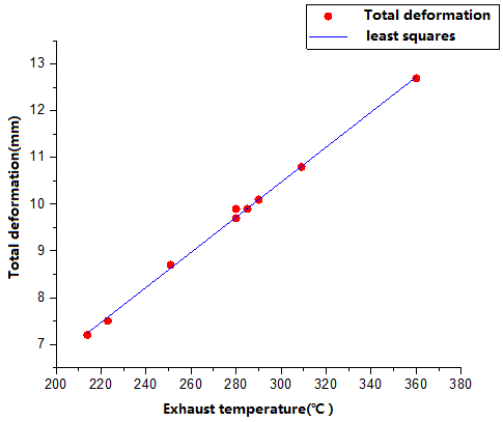

Figure 12 The relationship between the exhausttemperature and the maximum casing deformation

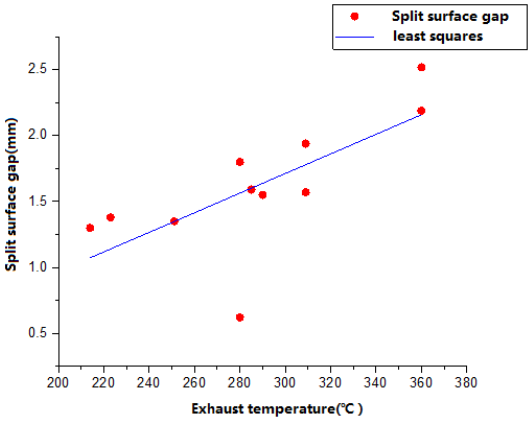

Figure 13The relationship between exhaust temperature and split surface gap

CONCLUSIONS

This paper uses ANSYS Workbench finite element software to analyze the structural strength and air-tightness of a large axial compressor casing. Specific analysis contents include casing temperature field distribution, casing static load, casing Thermal-solid coupling analysis, casing split surface air-tightness analysis, casing stress and deformation analysis under hydrotest, casing deformation without bolts.

The calculation results show that under the worst working conditions, the stress and deformation of most areas of the casing are within the allowable range; the position with the largest displacement is at the position of the air outlet flange of the high-pressure end, reaching 12.6mm. The stress value in most areas of the casing is below 350MPa, and the stress at the position of the high-pressure end where the endplate bears the rotor and the position of the root of the split surface in the supporting steel plate of the high-pressure end blade bearing cylinder is close to or exceeds 350MPa; most of split gap of the casing is within 1mm, and under the working conditions of the composite sealing strip, the gap value near the shaft hole of the high-pressure end may exceed 1mm.

According to the calculation results of ANSYS, the deformation, stress and split surface gap of the casing mainly depend on the temperature field distribution of the casing. The maximum overall deformation of the casing has a good linear relationship with the temperature of the exhaust port. The split surface gapis also positively correlated with the exhaust port temperature, but the regularity is slightly weaker. This is mainly due to the fact that the split surface gap is more sensitive to the setting of pressure, temperature and other boundary conditions, bolt pre-tightening force, component load and other factors, and the calculation is more difficult to converge.

The overall design layout of the compressor casing involved in the paper is reasonable, which can meet the strength and deformation requirements under various complicated working conditions. The pictures, figures and tables in the calculation results can provide a certain reference for future design.

REFERENCES

Dai. (2010). Analysis and optimum design of the nitric acid 4 in 1 unit foundation. Southwest Jiaotong University.

Ruan. (2007). Analyzing the security of the startup process of 600mw steam turbine is based on viral convection hot coefficient. North China Electric Power University (Beijing).

Yu. (2008). The analysis and research on hydrotest of weld casing in the compressor. Northeastern University.

Li, He, & Chen. (2011). Design, simulation and optimization of Ansys workbench (2nd edition). Beijing: Peking university press.
Chen. (2011). Study of high strength bolt joint on the wind turbine. Chongqing University.
Xie, Li, & Zhang. (2005). A numerical model for 3-d thermal elastic contact analysis and its application in the steamtight analysis of high-pressure casing of turbine. Mechanical Strength, 27(1), 95-8.
Su. (2005). A study on the heat transfer and the intensity of q475 engine body. Chongqing University.
Lv. (2008). Design & finite element analysis of ocean riser flange. Harbin Engineering University
GB50040-96. (2012). Code for design of dynamic machine foundation.